ORIGINAL ARTICLE

An adaptive framework for robotic polishing based on impedance control

Srinivasan Lakshminarayanan [1] · Sreekanth Kana [1] · Dhanya Menoth Mohan [1] · Omey Mohan Manyar [1,2] · David Then [2] · Domenico Campolo [1]

Abstract

Precise finishing operations such as chamfering and filleting are characterized by relatively low contact forces and low material removal. For such processes, conventional automation approaches like pre-programmed position or force control without adaptations are not suitable to obtain fine surface finishing with high profile accuracy. As a result, polishing tasks are still mainly carried out manually by skilled operators. In this paper, we propose an adaptive framework capable of polishing a wide range of materials including hard metals like titanium using a collaborative robot. We propose an iterative learning controller based on impedance control that adapts both position and forces simultaneously in each iteration to regulate the polishing process. The proposed controller can track the desired profile without any a priori knowledge of the forces required to polish different materials. In addition, we introduce a novel mathematical model to generate the complex filleting toolpath based on Lissajous curves. Trials are carried out in finishing tasks such as chamfering and filleting using a collaborative industrial robot to validate the novel framework. Surface roughness and profile measurements show that our adaptive controller can obtain fine polishing output in various materials such as titanium, aluminum, and wood.

Keywords Collaborative robots · Impedance control · Toolpath generation · Robotic polishing · Filleting · Chamfering

1 Introduction

Robotic research has witnessed remarkable advances in industrial applications such as spray painting, palletizing, and welding. Such tasks are performed using either simple position-based or force-based control strategies as the interaction between the end effector and the environment is negligible. Despite the numerous advancements in robotics, the tasks that involve physical interactions with the environment in which humans excel are inherently challenging for the robots to carry out autonomously. The subtle positional and force adaptations exhibited by the human operators to compensate for instabilities cannot be captured by pre-programmed position or force control strategies alone [1, 2]. As a consequence, polishing tasks that take up to 50% of total manufacturing time in the industry [3] still predominantly rely on skilled operators. Notwithstanding the growth, robot finishing constitutes less than 1% of current robot applications [4]. This is owing to several factors such as the robotic metal finishing still not as good as manual operation in the surface finish in smoothness, accuracy, and the difficulties in programming the robot itself. These problems are exacerbated when it comes to small and medium enterprises (SME) due to high mix low volume parts handled by them.

Robots that are used for polishing require a high degree of compliance during the execution to control the final output [5–10]. Thus, an adaptive interaction control is required to achieve the desired profile geometry and surface roughness which can be achieved based on either special compliant tools such as macro-mini systems or compliance based on the control algorithms. In the interaction control using special compliant tools, the end effector can typically compensate for force errors in different axes. The compliant tools can either be passive [11–13] or can be active tools [14] to maintain the desired contact force. The passive compliant tools usually rely on the compliance of the tool itself to maintain the normal contact

✉ Domenico Campolo
d.campolo@ntu.edu.sg

[1] School of Mechanical and Aerospace Engineering, Nanyang Technological University, Singapore 639798, Singapore

[2] Rolls-Royce Plc, Singapore, Singapore

force, whereas the active tools rely on a closed-loop force control system to correct the force errors. Huang et al. in [11, 13] make use of passive compliant tools (PCT) for grinding and polishing turbine vanes. In [15], an active end effector–based force control system is devised for robotic deburring. Although the active compliance control that uses an actuator is very good resulting in high accuracy, there are difficulties in designing these special compliant polishing tool [16]. Further, excessive compliance of the tool will decrease the stiffness during the polishing and makes the profile tracking less accurate.

To achieve interaction tasks using control algorithms, either hybrid position/force controllers or impedance controllers are typically deployed. In a hybrid position/force control for surface finishing, the position is generally regulated along the surface, while the force is usually controlled in normal directions. Force control strategies and hybrid position/force control of robotic manipulators have been extensively deployed for finishing processes including deburring, polishing, and grinding. A comprehensive overview of robot force control can be found in [17, 18]. In [19], hybrid position/force control based on fuzzy control is proposed for obtaining the desired chamfer depth. Surdilovic et al. [20] utilized CAD/CAM for path planning for milling and grinding very hard materials like Inconel and proposed a combination of force and feed control for polishing hard materials. Hybrid control requires precise knowledge of surface geometry to yield a good surface finish. Besides, as a controller with fixed impedance, hybrid control struggles with stability issues arising from tool usage [21] and cannot adapt to unknown surface conditions.

In impedance-based control, the relationship between the position and force is regulated, thus enabling to adapt to unknown environments. Hogan [22] in his seminal work proposed the idea that, in impedance control, the force commanded to the robot is regulated in response to a variation of the nominal trajectory (due to the interaction with the external environment), while in admittance control, the robot kinematics is controlled in response to a detected force (arising from the interaction with the environment). In a pioneering work, Kazerooni [23] developed and implemented impedance control methodology for precision deburring and grinding. Later, Wang et al. [24] developed an adaptive framework based on impedance control in which the cutting force and feed rate are adjusted automatically to obtain better quality, in which a model is developed to predict the cutting force. Isela et al. [25] were able to perform path tracking maneuvers using impedance control on industrial robots. Loris et al. [26] performed robot probing tasks by limiting the force overshoots in which the control gains are defined analytically by estimating environment stiffness using an extended Kalman filter. Drawing inspiration from human behaviors, Yanan et al. [27] presented a human-like controller to interact with unknown environments that can adapt force, stiffness, and position for contact tasks such as drilling and cutting.

Furthermore, Buckmaster et al. [4] proposed an admittance control–based approach for surface finishing in which a high admittance is maintained normal to the part surface and high impedance is maintained tangent to the part surface where the tool path is generated using CAD, which is similar to the hybrid position/force control.

One of the robust control schemes involves iterative learning control (ILC) which is simple to implement and does not require exact knowledge of the dynamic model of the robot [28, 29]. In a typical iterative impedance control scheme for a robotic manipulator, the control objective is to track a target (reference) impedance model as well as the reference trajectory, in which the impedance is learned [30–32]. Such an ILC ensures that the system response fulfills the specified target impedance as the actions are repeated.

Despite these advancements, finishing remains challenging and is an active research problem [33–40], especially difficult due to the double whammy of dealing with instabilities from chattering as well as the difficulty in achieving precision in polishing hard materials for numerous industrial applications. Our goal in this study is to develop a complete framework that can carry out the finishing operations on a variety of materials using collaborative robots in a simple yet robust manner suitable for SME. We propose a novel iterative learning controller based on impedance that simultaneously adapts both the position and the force in each iteration. Unlike the iterative adaptive impedance controllers found in the literature [28, 30–32], the proposed iterative controller does not require any a priori knowledge of forces to polish a particular material and does not require force feedback as the force adaptation is accomplished implicitly.

We validate the adaptive controller through various chamfering and filleting trials on numerous materials such as titanium, aluminum, and wood. In addition to the robot control, manual programming of the robot is highly cumbersome and needs highly skilled operators [41]. Since the polishing posture and the toolpath have an enormous effect on the efficiency of the overall polishing operation as well on the surface integrity of the workpiece [16], SMEs often have to rely on either inefficient manual programming or expensive vision sensors [42]. To address this challenge, we propose a novel mathematical model to generate a toolpath in real time for filleting process based on Lissajous curves that do not require any external sensors. Further, our framework extensively utilizes kinesthetic teaching in low impedance settings through which an operator can intuitively teach various processes efficiently.

Major contributions of this paper include a robust ILC based on fixed impedance to track the position and to implicitly control the force to polish different materials, including hard metals like titanium, using collaborative robots and the mathematical model to generate the filleting toolpath. One of the main advantages of our framework is that the no

Table 1　Nomenclature

X′,Y′,Z′	Coordinate axes
θ	Tool inclination
A,B	Amplitude of the functions Y′ and θ, respectively
a,b	Frequency of the functions Y′ and θ, respectively
δ	Phase shift between the functions Y′ and θ
t, t_i	Time associated with functions Y′ and θ and sampling time, respectively
R	Fillet radius
$\mathbf{X}_{REF}$, $\mathbf{X}_{CMD}$, $\mathbf{X}_{ACT}$	3D positions in reference, commanded and actual trajectory in mm respectively
R	Orientation
P	6D via frame consisting position X_P and orientation R
P_{REF}, P_{CMD}, P_{ACT}	6D frame in a reference, commanded and actual trajectory, respectively
T_{REF}	Reference trajectory comprising sequence of via frames P_{REF}
T_{CMD}	Commanded trajectory comprising sequence of via frames P_{CMD}
T_{ACT}	Actual trajectory comprising sequence of via frames P_{ACT}
Λ	Inertia matrix of the robot
D_d	Desired Cartesian damping
K_d	Desired Cartesian stiffness
$\mathbf{W}_{ext}$	External wrench vector comprising the force and torques
$\mathbf{f}_{ext}$, $\boldsymbol{\tau}_{ext}$	External forces and torques
M	Number of via frames P in a trajectory
N	The number of iteration/pass
ε_P	Kinematic positional error between two via frames
α	Proportional gain for positional error
$\delta \mathbf{P}$	Auxiliary positional error

knowledge of the force is required as a priori to polish parts made of different materials, which is particularly helpful for SMEs that process high mix low volume workpieces. Further, our framework can acquire the toolpath and posture efficiently without requiring any additional force sensors or vision systems keeping the cost of the entire setup economical and at the same time overcome the bottlenecks associated with manual programming. To the authors' knowledge, we are the first to study polishing using cobots based on an iterative impedance controller and propose an accurate way to generate a toolpath for filleting in real time.

The paper is organized as follows: In Section 2, the mathematical model to generate the toolpath and the iterative controller are introduced. In Section 3, the hardware and the software setup for the polishing trials are described. Using the chamfering trials on titanium workpieces as a use-case, we provide an elaborate account on the effects of the proposed controller in Section 4.1. To illustrate the generalization capability of the proposed framework on different materials, the trials on aluminum coupons are explained in Section 4.2, and in Section 5, the filleting trials on aluminum and wood are briefly outlined.

2 Toolpath generation and adaptive controller

The toolpath generation for chamfering and filleting process is described in Section 2.1. Further, the details on the proposed adaptive controller are given in Section 2.2. The nomenclature of the symbols used in the article is given in the Table 1.

2.1 Toolpath generation

To generate the reference trajectory for the robot quickly without requiring any vision systems, we utilize kinesthetic teaching by the operator. The details of the toolpath generation for chamfering and filleting process are described in Sections 2.1.1 and 2.1.2, respectively.
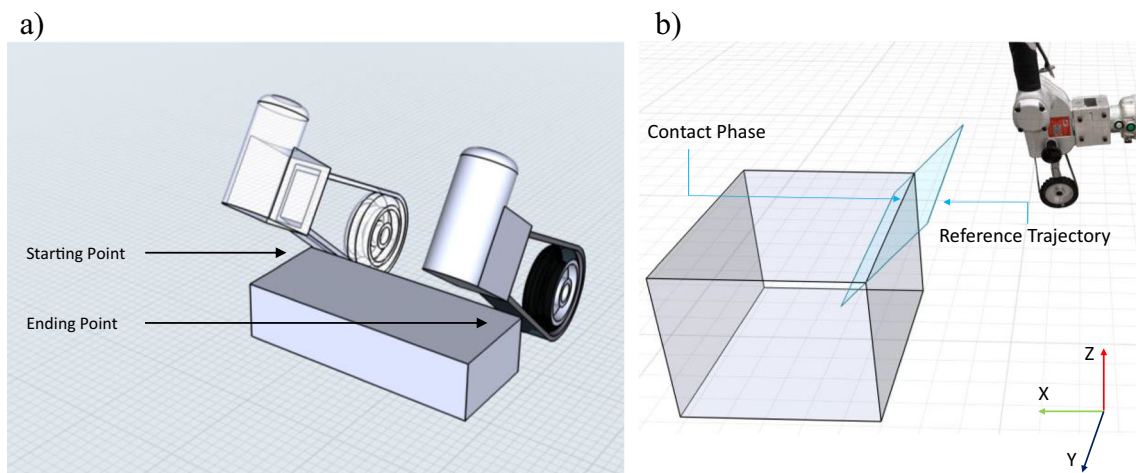

Fig. 1　**a** Kinesthetic teaching and **b** illustration of the chamfering trajectory
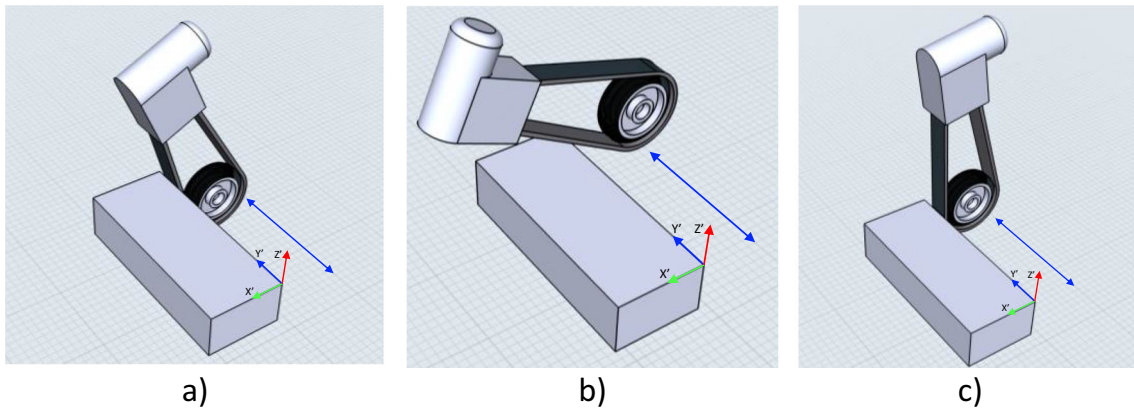
Fig. 2 Varying tool poses in filleting (**a**) at the edge, (**b**) X′Y′ face, and (**c**) Y′Z′ face

### 2.1.1 Toolpath generation for chamfering

Chamfering is a finishing operation in which a sharp edge is beveled generally at an angle of 45° to the two adjoining right-angled faces. For obtaining the toolpath for the chamfering, in our framework, the human operator kinesthetically teaches the robot in a low impedance (high compliance) mode (i.e., with stiffness values as low as 1 N/m, whereas maximum achievable values are as high as 5000 N/m). Using the starting and ending points of the

chamfering and the robot posture obtained from the kinesthetic teaching by the operator, a reference trajectory is generated by linear interpolation with a user-specified chamfering depth as illustrated in Fig. 1a and b.

2.1.2 Toolpath generation for filleting based on a mathematical model

Filleting is a polishing process of rounding an edge to improve the part's durability by dispersing the stress concentration.

Fig. 3 **a** 2D Lissajous curves and **b** mathematical model to transform Lissajous into 3D Pose
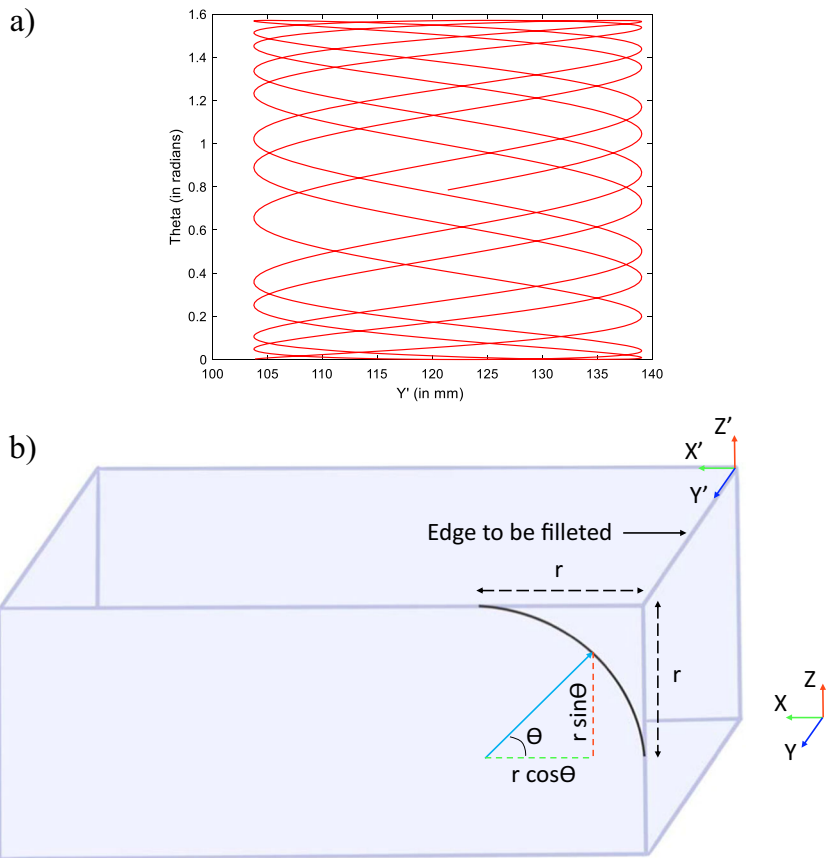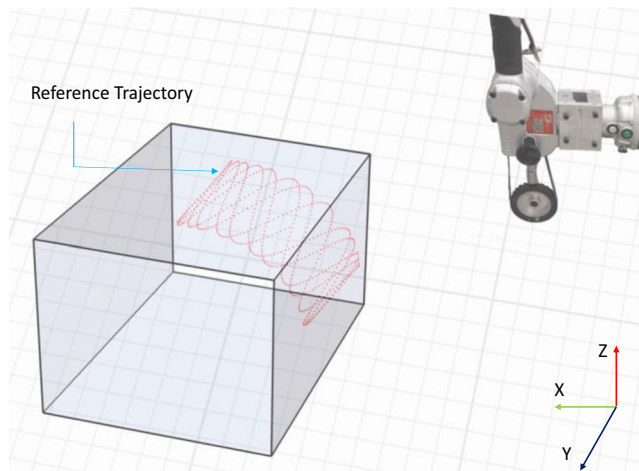
Fig. 4 Illustration of filleting trajectory

Unlike chamfering, the toolpath for the filleting is quite complicated due to the fact that the filleting trajectory requires fine motion with continuous changes in both position and orientation of the tool along the edge. In a typical industrial setting, the manual filleting process is carried out with two unique
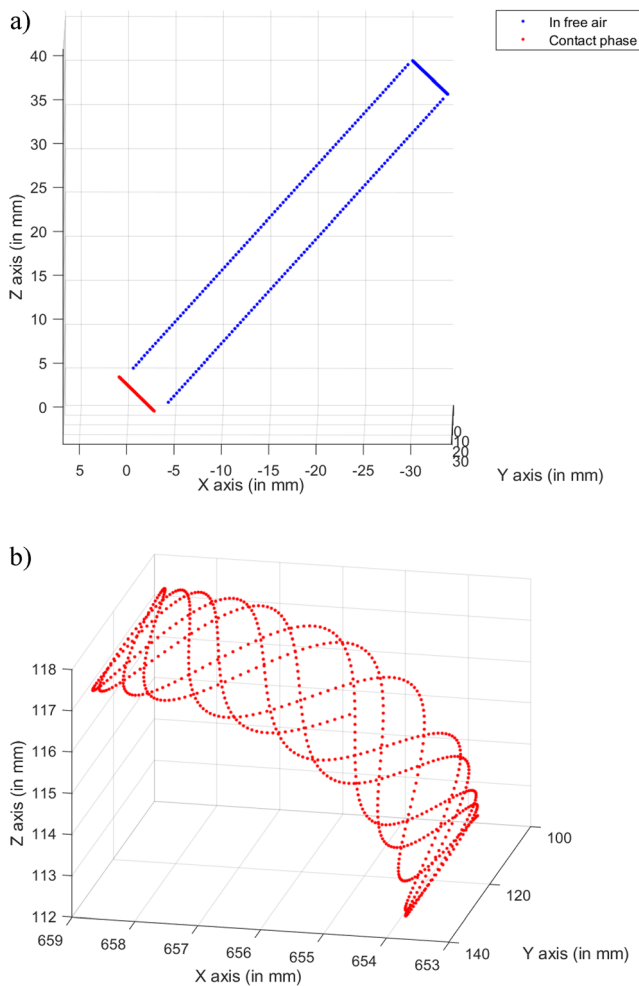

Fig. 5 Reference trajectory with via frames. **a** Chamfering and **b** filleting

features: the orientation of the tool is continuously varied and subsequently followed up by a lateral movement along the edge as shown in Fig. 2 to ensure that the edge is rounded off evenly. Inspired by both the manual filleting and chamfering process, we have reformulated the problem of filleting as a special case of chamfering in which the tool inclination is varied at different parts of the edge.

For example, when working exactly on the edge, i.e., the intersection between the two faces X′Y′ and Y′Z′, the tool will be at an inclination angle of 45° as observed from the Fig. 2a. Further, when the tool is at the face X′Y′, the inclination of the tool θ will be increased depending on how far the tool center point is from the edge as indicated by Fig. 2b. At its farthest, the tool will be held parallel to the surface X′Y′ and θ = 90°. Likewise, when the tool is at the surface Y′Z′, the angle of inclination θ will be reduced depending on how far the tool center point is from the edge as viewed from Fig. 2c. At the extreme point, the tool will be at an upright vertical position on the face Y′Z′ and the θ = 0°.

The frames X′, Y′, and Z′, as shown in Figs. 2a, b, and c and 3b, are used to generate 2D Lissajous curves based on the kinesthetic teaching by the user and have an identical orientation to the robot's X, Y, and Z frames. To obtain a filleting toolpath in real time based on this strategy, we propose a simple mathematical model in which the two parameters angle of inclination θ and lateral movement along Y' are automatically generated using the concept of Lissajous curves [43]. In general, the Lissajous is the 2D wave patterns that are generated when we plot two sinusoidal waves on both X- and Y-axes as indicated by the Eqs. (1) and (2).

$$Y' = A\sin(at + \delta) \tag{1}$$
$$\theta = B\sin(bt) \tag{2}$$

where A and B refer to the amplitude of the functions Y′ and θ, respectively; a and b refer to the frequencies of the functions Y′ and θ respectively; and δ refers to the phase shift between the functions Y′ and θ. By modifying the frequency, amplitude, and phase shift, we can generate a wide variety of patterns for disparate application. Using the starting and ending poses P_1 (x_1, y_1, z_1, R_1) and P_2 (x_2, y_2, z_2, R_2), respectively, as well as the desired fillet radius (r) that is obtained from the user, a 2D Lissajous curve is generated using two functions Y′ and θ [Eqs. (3) and (4)] as shown in Fig. 3a.

$$Y' = \frac{(y_2 + y_1)}{2} + \left(\frac{y_2 - y_1}{2}\right)\sin(at + \delta) \tag{3}$$
$$\theta = \frac{\pi}{4} + \left(\frac{\pi}{4}\right)\sin(bt) \tag{4}$$

The terms $(y_2 + y_1)/2$ and $\pi/4$ are added to functions Y′ and θ, respectively, to ensure that resultant filleting motion is
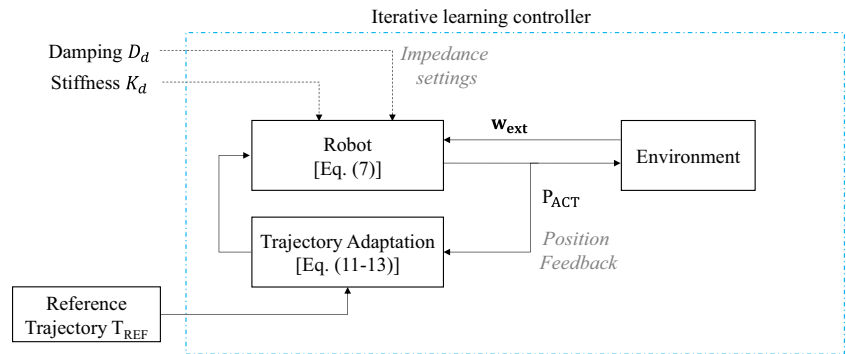
smooth with continuous changes in both position and orientation of the tool along the edge as shown in the Fig. 2. As we need the reference trajectory comprising 3D poses to command the robot, a relationship between 2D Lissajous pattern to the 3D position is established based on the model as illustrated in Fig. 3b.

Using the desired fillet radius and Y' and θ that we generated using the 2D Lissajous curves, the position component of the pose X_P and the rotational component R are determined as follows.

$$X_P = \begin{bmatrix} r - r\cos\theta \\ Y' \\ -(r - r\sin\theta) \end{bmatrix} \tag{5}$$

$$R = \begin{bmatrix} \sin\theta & 0 & -\cos\theta \\ 0 & 1 & 0 \\ \cos\theta & 0 & \sin\theta \end{bmatrix} \tag{6}$$

Thus, using the Eqs. (5) and (6), the 2D Lissajous curve in the parametric space is transformed into the 3D poses for the
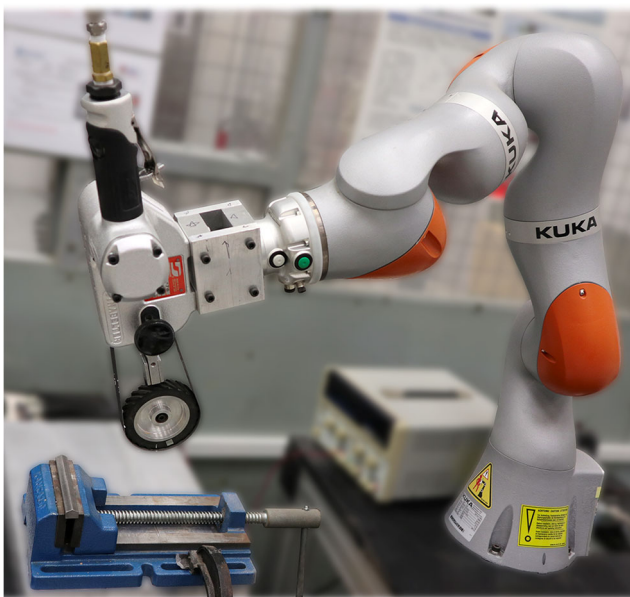

Fig. 7 KUKA iiwa R800 Robot attached with abrasive belt tool

reference robot trajectory. As the orientation directly obtained from the Eq. (6) changes at each successive point which may lead to jittery motion of the tool, we fixed the filleting orientation by using 8 discrete sets of angle θ between 0° and 90° by rounding off the angles R obtained from Eq. (6) and thus generated a reference trajectory to yield a fillet profile with desired radius (r) as illustrated in Figs. 4 and 5b. Reference trajectories for both chamfering and filleting are used to initialize the robot motion, and once a reference trajectory is generated, any interaction with the human operator is no longer required.

2.2 Iterative controller based on impedance

In our iterative learning controller based on impedance, the robot acts as a virtual spring-damper system in which the force exerted on the environment is directly proportional to the difference between the desired state of the robot and the actual state. The dynamics of an impedance-controlled robot in Cartesian space, from Ficuciello et al. [44], is given by

$$\Lambda\ddot{P}_{ACT} + D_d\left(\dot{P}_{CMD} - \dot{P}_{ACT}\right) + K_d(P_{CMD} - P_{ACT}) = \mathbf{W}_{ext} \tag{7}$$

where Λ represents the 6 × 6 inertia matrix of the robot and the P_{CMD} and P_{ACT} are the 6D configuration frames that represent the commanded and the actual pose of the robot that include 3D positions X_P and orientation R in Euler angles. In general, a robot pose P can be represented as shown in the equation below.

$$P = \begin{bmatrix} \mathbf{X_P}^T & R^T \end{bmatrix}^T \tag{8}$$

The matrices D_d and K_d are the desired Cartesian damping and desired Cartesian stiffness matrices, respectively, both being 6 × 6 matrices. The term $\mathbf{W}_{ext}$ represents the external interaction wrench arising from the tooling task and includes both interaction 3D forces $\mathbf{f}_{ext}$ and 3D torques τ_{ext}, i.e., $\mathbf{W}_{ext} = [\mathbf{f}_{ext} \ \tau_{ext}]^T$.

To make it specific about the position, consider an initial trajectory of the robot T_{REF} which comprises of M "via"

frames P, each with position $\mathbf{X}_P$ and orientation R and with the sampling time t_i in milliseconds. The reference trajectory T_{REF} for chamfering and filleting can be represented as a sequence of robot pose frames P as shown in Fig. 5a and b, respectively. The chamfering reference trajectory is comprised of 400 via frames with a user-specified chamfer depth of 1 mm, while the filleting reference trajectory includes 800 via frames with a user-specified fillet radius of 5 mm.

$$T_{REF} = \{P_{REF}(t_i), i = 1, 2, \ldots, M\} \qquad (9)$$

Similarly, a commanded trajectory for any pass can be written in terms of frames P as,

$$T_{CMD}^N = \left\{P_{CMD}^N(t_i), i = 1, 2, \ldots, M\right\} \qquad (10)$$

where the subscript N represents the iteration number and, for the first iteration, the commanded trajectory of the robot will be equal to the reference trajectory $T_{CMD}^1 := T_{REF}$. The commanded frames of the end effector are represented as $P_{CMD}^N(t_i)$, while the actual frames of the end effector are represented as $P_{ACT}^N(t_i)$. Kinematic positional error ε_P is determined by the following equations:

$$\varepsilon_P^N(t_i) = \mathbf{X}_{REF}(t_i) - \mathbf{X}_{ACT}^N(t_i) \qquad (11)$$

$$\delta\mathbf{P}^N(t_i) = \alpha * \varepsilon_p^N(t_i) \qquad (12)$$

where both $\varepsilon_p^N(t_i)$ and $\delta\mathbf{P} \in \mathbb{R}^3$ are used to track the desired reference trajectory, N indicates the iteration number, and α is the proportional gain. The actual position of the robot at each instance of time t_i is then measured using the in-built robot sensors and subsequently sent to the MATLAB for analysis. For the next iteration $N + 1$, the commanded trajectory of the robot will be computed as follows:

$$T_{CMD}^{N+1} = \left\{\left[\left(\mathbf{X}_{CMD}^N(t_i) + \delta\mathbf{P}^N(t_i)\right)^T R(t_i)^T\right]^T, i = 1, 2\ldots, M\right\} \qquad (13)$$

Intuitively, it can be interpreted that the commanded trajectory is iteratively adapted so that robot actual trajectory can track the desired reference trajectory resulting in the desired geometric profile of the workpiece. The advantage of using iterative impedance control in interactive tasks is that the force would automatically adapt depending on the relationship with the position. Thus, the proposed algorithm adapts the positions directly while implicitly controlling the contact force. From Eq. (7), The force exerted by the manipulator is directly proportional to the difference between the commanded position and actual position, i.e.,

$$\mathbf{f}_{ext} \propto (\mathbf{X}_{CMD} - \mathbf{X}_{ACT}) \qquad (14)$$

The controller that we propose for the polishing processes accomplishes the whole operation in multiple iterations (passes). Based on the Eqs. (11), (12), and (13), both position and forces are adapted iteratively in each pass. As the tool center point of the robot is required to be a maintained at a certain orientation in the chamfering and filleting processes, we consider only the adaptation of the position of the frames in the control algorithm in Eqs. (11), (12), and (13); i.e., only the positional component $\mathbf{X}_P$ will be adapted, and orientation R will be kept constant. If the tool is not removing enough material and still far from the reference position (i.e., high value ε_P^N) in the Nth iteration, the force $\mathbf{f}_{ext}$ would increase in the subsequent N + 1th iteration to facilitate higher material removal. Similarly, if the tool removes the material adequately and the difference between the commanded and actual positions is low (i.e., low ε_P^N), the corresponding interaction force tends to be low in the next N + 1th iteration. Thus, the robot operator does not need any a priori information about the contact forces required to polish a material. Though the actual trajectory of the robot can converge with the initial reference trajectory given enough time, we achieved the best results in chamfering and filleting with 15 and 5 iterations, respectively, from our trials. The steps involved in chamfering and filleting can be illustrated as below.

The feedback about the actual position, forces, and

Algorithm: Steps involved in Chamfering
1: Initiate the robot in a compliant mode
2: Kinesthetic Teaching of the starting and ending points of chamfer
3: Generation of the desired robot Trajectory T_{REF} with user-specified chamfering depth
4: **Repeat:**
5:     Initiation of robot motion for the Nth pass
6:     Continuous measurement of robot poses during the motion
7:     After end of pass N, Calculation of ε and δ for each via frame based on T_{ACT}^N
8:     Determination of new commanded trajectory T_{CMD}^{N+1} for next $(N+1)^{th}$ pass
9: **Until:** 15 passes based on Trial and Error

Algorithm: Steps involved in Filleting
1: Initiate the robot in a compliant mode
2: Kinesthetic teaching of the starting and ending points of fillet
3: Generation of the desired robot Trajectory T_{REF} with user-specified fillet depth using the proposed mathematical model
4: **Repeat:**
5:     Initiation of robot motion for the Nth pass
6:     Continuous measurement of robot poses during the motion
7:     After end of pass N, Calculation of ε and δ for each via frame based on T_{ACT}^N
8:     Determination of new commanded trajectory T_{CMD}^{N+1} for next $(N+1)^{th}$ pass
9: **Until:** 5 passes based on Trial and Error

orientation with which the robot reaches any particular point is logged and stored for analytical purposes. At the end of each iteration, the actual trajectory obtained from the controller is compared with the reference trajectory in Eq. (11) and subsequently used to adapt the commanded trajectory in Eq. (13) to diminish the positional error in the next iteration as shown in Fig. 6. Such an incremental adaptation of trajectory is to ensure that the finishing operation is accomplished following the desired profile and incremental force adaptation without damaging the workpiece. Furthermore, due to the error correction through an iterative feedback, loop also lessens the amount of rework later.

The proposed controller is very different from a typical position-based impedance control approaches found in the literature [45, 46]. In a typical position-based impedance control, an inner positional control loop is combined with an outer force control loop. The inner loop represents a common positional controller, while the outer loop includes a force

feedback compensator representing admittance. This outer loop becomes active when the end effector contacts environment and induce a force. Based on the force error between the actual force and target force, the force compensator produces a position adjustment command. In the inner loop, the position error is used to induce the force (impedance) by multiplying with a given stiffness value (K). Unlike a position-based impedance controller, our proposed controller does not require force feedback compensator to simultaneously adapt the force and trajectory.

3 Experimental setup

3.1 Hardware setup

The hardware structure consists of KUKA LBR iiwa 7 R800 compliant robot that uses Series Elastic Actuators to actuate the

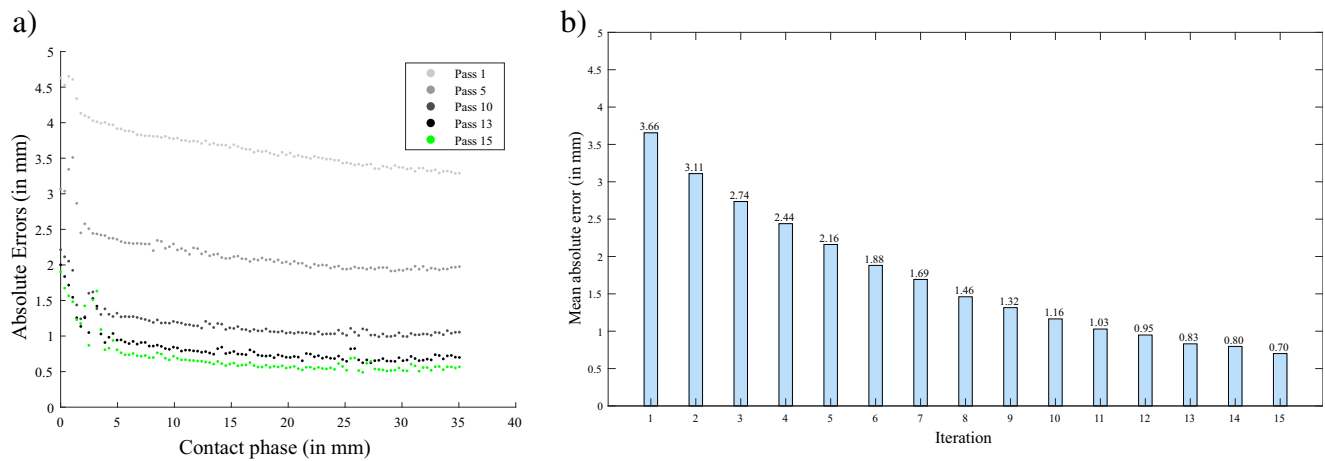Fig. 8 a Commanded and b actual path followed by the robot
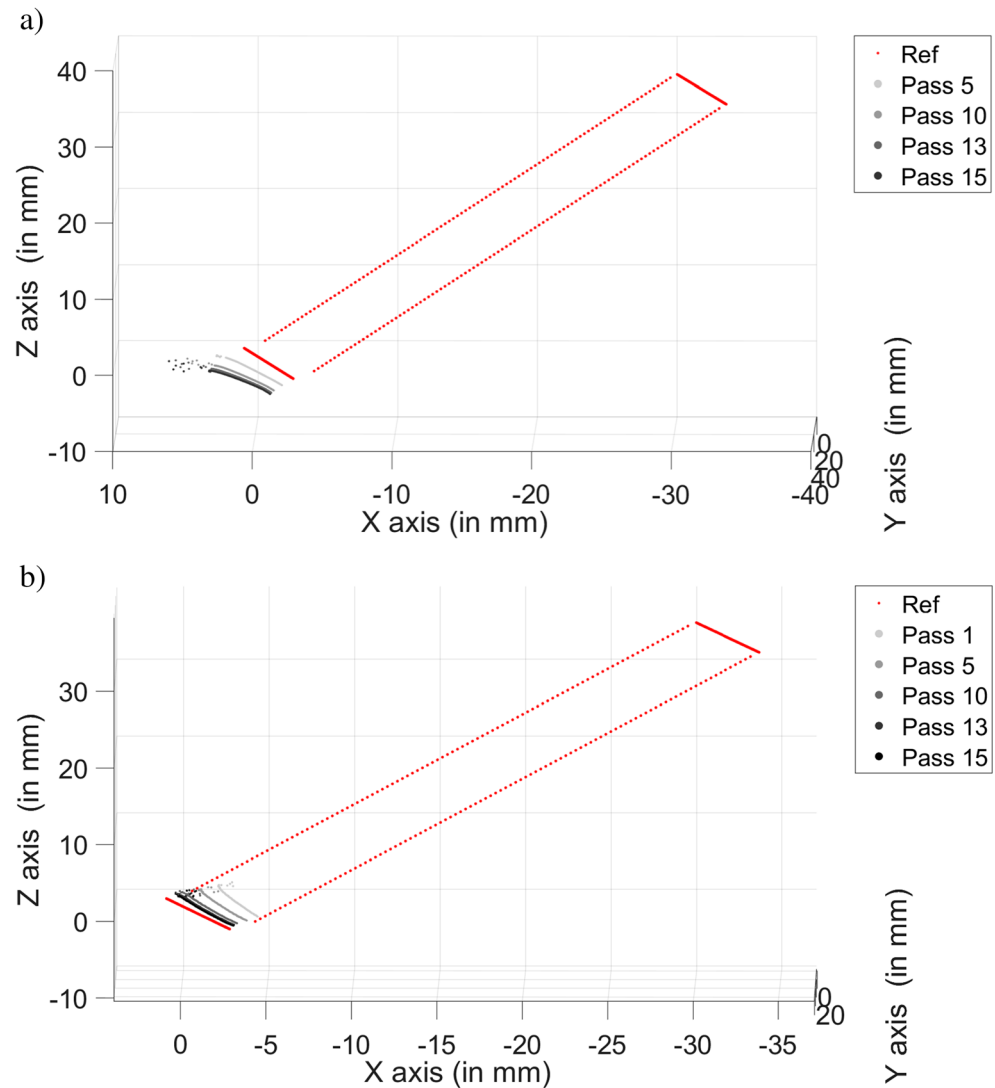
Fig. 9 **a** Absolute error and **b** mean absolute error between T_{REF} and T_{ACT}

joints. It possesses 7 degrees of freedom, has 7 kg payload, and has a repeatability of ± 0.1 mm. As a result of its low weight, it has a low moment of inertia which makes the robot adept in responding to collisions to minimize its impact and is ideal for collaborative tasks involving humans. A Dynabrade 11476 dynabelter abrasive belt tool powered by compressed air is attached to the flange of the KUKA robot as shown in Fig. 7. This Dynabrade tool is a heavy-duty model with 1″ wide abrasive belt capacity and hence capable of polishing even the metals with very high hardness such as titanium. We used an abrasive of grit size P100 for the chamfering trials on both titanium and aluminum coupons and the filleting trials on aluminum workpieces. The KUKA robot supports impedance control mode, which is ideal to carry out collaborative tasks and to ensure a robust response to environmental uncertainties. In impedance mode, the linear stiffness can be set up to 5000 N/m, while rotation stiffness can be set up to 300 Nm/rad.

3.2 General software architecture

The KUKA robot is programmed with Sunrise Workbench software based on JAVA Programming language using KUKA RoboticsAPI with its predefined methods. Using the TCP/IP connection, a bidirectional communication link between MATLAB and Sunrise Workbench is established. We used an in-built mode in Sunrise Workbench known as "Sunrise Connectivity Servoing" that can set one end destination frame for the KUKA robot at a time from MATLAB. By updating the end destination continuously in real time from MATLAB, a continuous stream of Cartesian trajectory is given to the KUKA robot. During the robot execution, the actual pose of the robot for each via frames is measured and sent back to MATLAB for iterative adaptation. Thus, at the end of each pass, the actual trajectory followed by the robot is determined through the feedback from the controller and compared against the
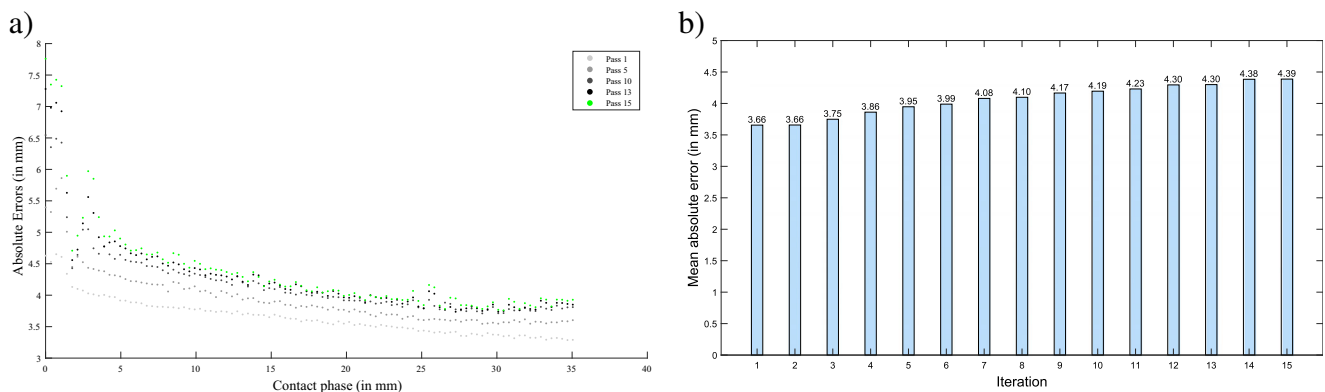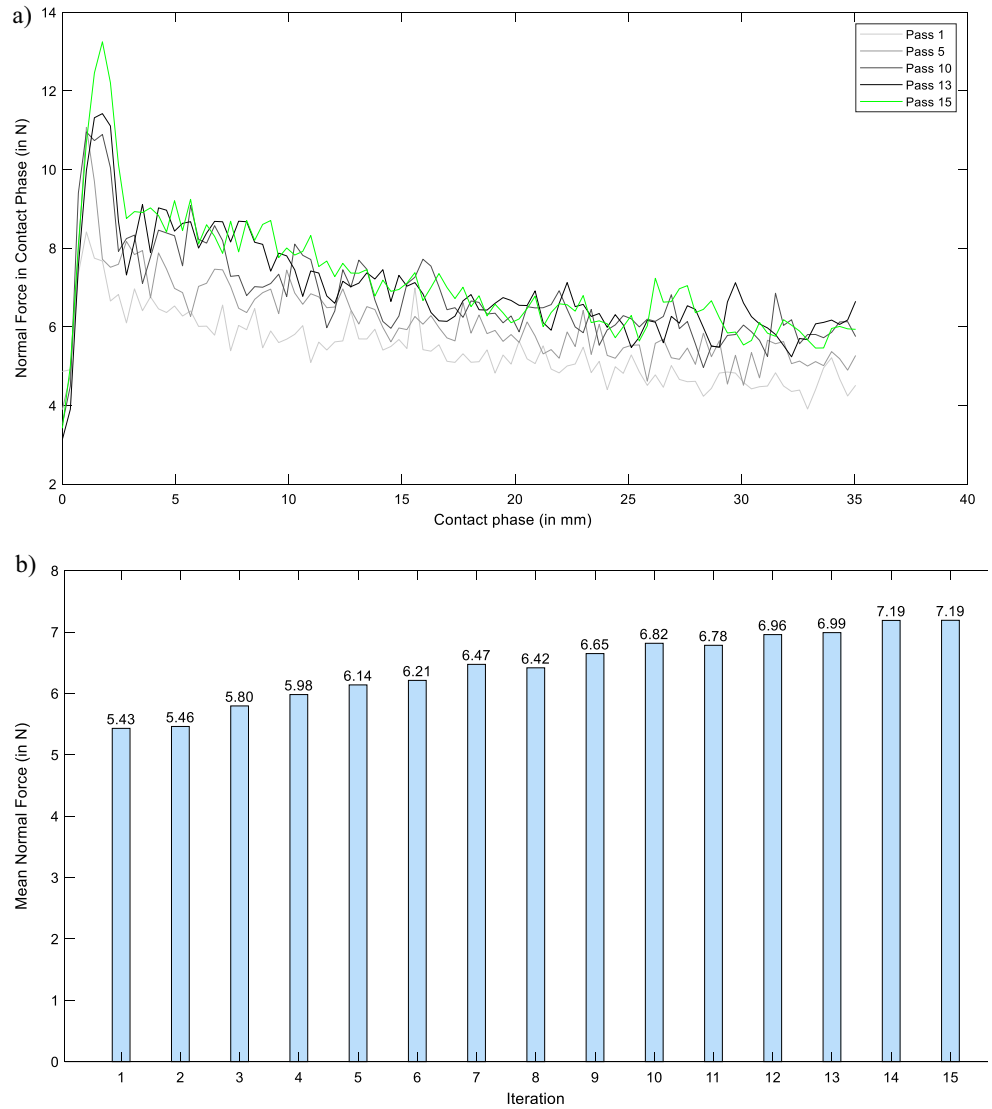

Fig. 10 **a** Absolute error and **b** mean absolute error between T_{CMD} and T_{ACT}

Fig. 11 **a** Normal forces and **b** mean normal forces chamfering titanium workpieces

reference trajectory using the adaptation algorithm proposed in Section 2.2 and consequently used to update the commanded trajectory in the next iteration.

For the experiments on the chamfering and filleting, the stiffness matrix K_d is set such that the translational stiffness along X-, Y-, and Z-axes is 800 N/m, while the rotational
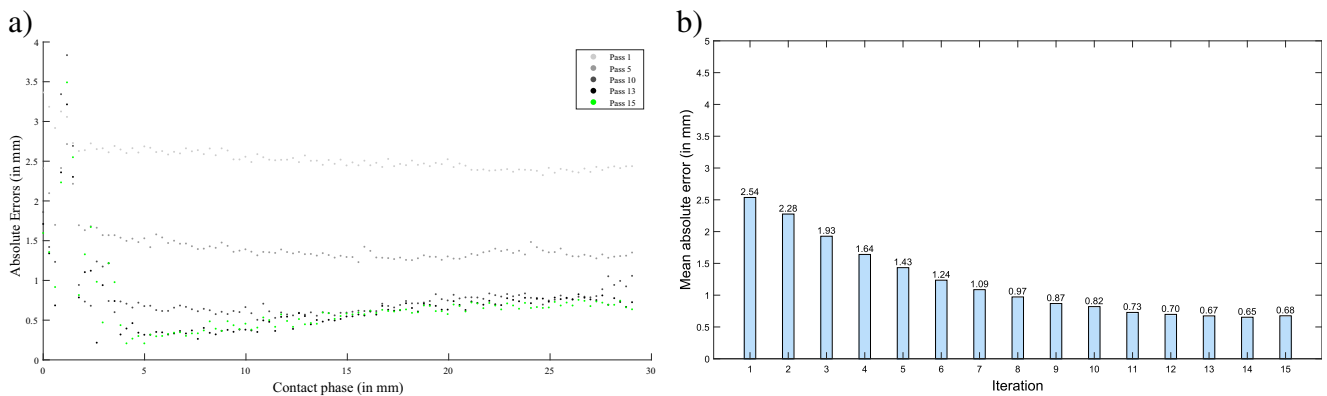

Fig. 12 **a** Absolute error and **b** mean absolute error between T_{REF} and T_{ACT}
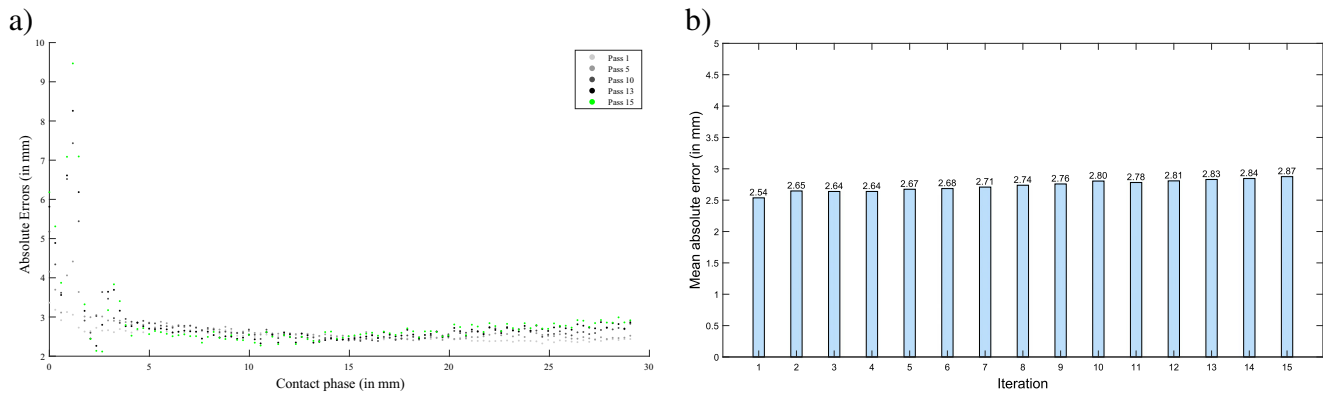
a)

b)

Fig. 13 **a** Absolute error and **b** mean absolute error between T_{CMD} and T_{ACT}

stiffness about all axes is set to 300 Nm/rad. The value of the damping coefficient (D_d) for all degrees of freedom is set at 0.7.

4 Experiments on chamfering

We selected titanium and aluminum coupons for the chamfering trials as they are among the widely used materials in the manufacturing industry. The effects of the iterative controller are described in detail in Section 4.1 taking the chamfering trials on titanium workpieces as a use-case. In addition, the results of the trials on aluminum work coupons are briefly explained in Section 4.2. Finally, the profile and surface roughness measurements of the chamfered components are provided in Section 4.3.

4.1 Chamfering trials on titanium workpieces

Based on the kinesthetic teaching of the robot in a compliant mode, we first obtained the reference trajectory for chamfering with a chamfer depth of 1 mm in both X and Z directions as viewed in Fig. 5a. Subsequently, the chamfering trials on titanium work coupons are initiated with a gain of around 15% (i.e., $\alpha = 0.15$) in the Eq. (12). Once an iteration is complete, the actual trajectory followed by the robot is compared against the reference

trajectory of the robot and the commanded trajectory for the subsequent pass is adapted based on Eqs. (11), (12), and (13). Before the commencement of the operation, the commanded path at the first iteration equals the initial reference trajectory as observed from Fig. 8a. As the robot initiates the finishing operation in the first iteration, there was a positional difference between the reference and the actual trajectories of the robot despite the material removal. To overcome this positional error, the commanded position in X- and Z-axes are adapted significantly, attempting to go far deeper into the workpiece than the initial 1 mm depth given in the reference trajectory. The positional error between the reference and the actual trajectories of the robot keeps diminishing gradually after each iteration. This can be seen from plotting the actual path of the robot as shown in Fig. 8b. Further, the absolute error is computed for each instance of time by calculating the squared error between the reference and the actual trajectories of the robot as given below.

$$E_{abs} = \sqrt{\left((x_{REF}-x_{ACT})^2 + (y_{REF}-y_{ACT})^2 + (z_{REF}-z_{ACT})^2 \right)}$$

where x_{REF}, y_{REF}, and z_{REF} refer to the x, y, and z values of frames in reference robot trajectory (in mm) and x_{ACT}, y_{ACT}, and z_{ACT} refer to the x, y, and z values of frames actual robot
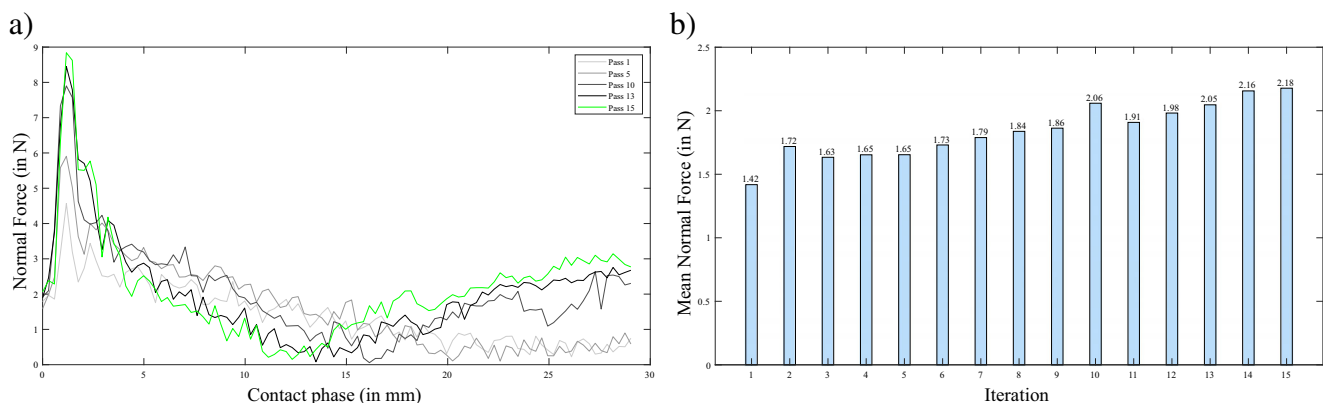
a)

b)

Fig. 14 **a** Normal forces and **b** mean normal forces chamfering in aluminum work coupons

Table 2 Profile measurement of the chamfered workpiece

S. no	Target chamfer depth (mm)	Actual depth (mm)		Accuracy (mm)		Reference accuracy from literature (mm)
		In titanium	In aluminum	Ti	Al	
1	1.00	0.86	0.98	± 0.133	± 0.033	± 0.3 [47]
2	1.00	0.87	1.02			
3	1.00	1.13	1.06			

trajectory (in mm). When we plot the absolute error (for each frame) and the mean absolute errors (for an iteration) between the reference and actual trajectories of the robot as in Fig. 9a and b, respectively, we observed the positional error keeps decreasing gradually after each iteration. We observed that the error reduction is significant in the initial passes followed by gradual plateauing in the later passes. Intuitively, this whole reduction in the positional error can be construed as a mechanism to track the required profile (i.e., reference trajectory) accurately after each pass, which is quite apparent from the lower values of the plot for the absolute errors.

As expected, the force exerted by the robot is highly dependent on the positional difference between the *commanded* (T_{CMD}) and the *actual trajectories* (T_{ACT}) at a given time instance as observed from the corresponding plots of absolute error and mean absolute error in Fig. 10a and b, respectively. Unlike the positional error between the *reference* and *actual trajectories*, this error is observed to be increasing after each subsequent adaptation. This has to do with the fact that robot is not able to reach the commanded path in the initial iteration, i.e., not able to penetrate the titanium workpiece to track the commanded path, and thus adapts its commanded path further to compensate for the low material removal and low forces. Thus, the forces are implicitly controlled by adapting the *commanded trajectory* in our controller.

Consequently, the normal force is initially low in the first few iterations as the force exerted on the workpiece by the robot is directly proportional to the positional difference between the *commanded* and the *actual trajectories* of the robot based on a virtual spring-damper system. As the commanded path gets adapted based on the positional error, the normal force also gradually updated after each pass as observed from Fig. 11a and b. During the initial pass, the mean normal contact

force is 5.43 N, and in the 15th pass, it reaches 7.19 N. In the force plots as observed from Fig. 11a, a significant spike in force is observed when the tool initially establishes contact with the workpiece.
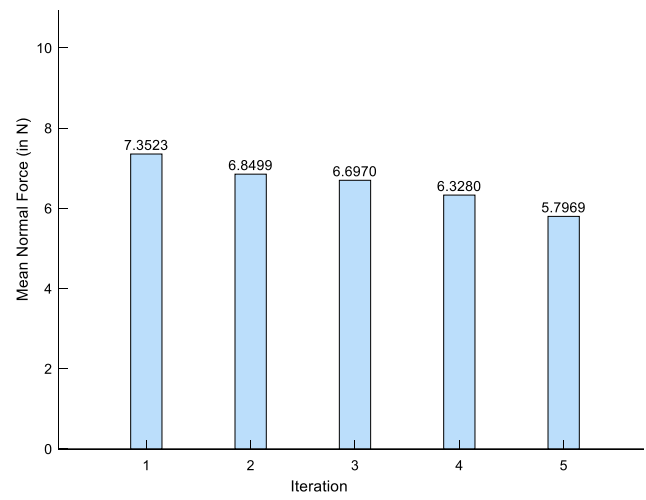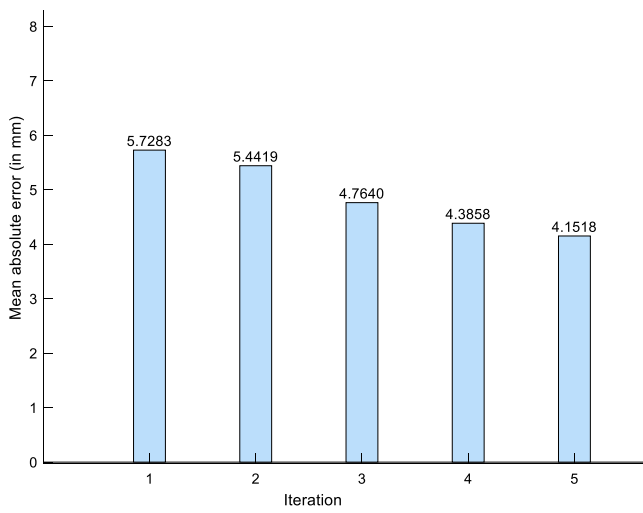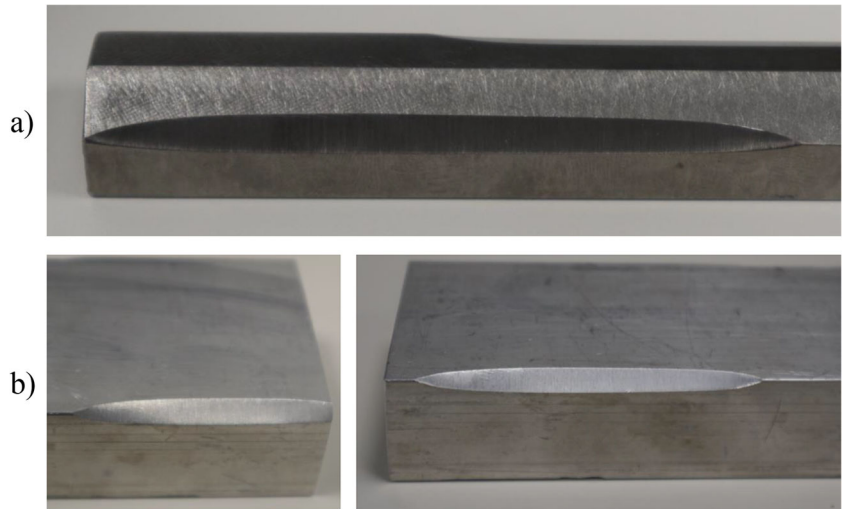
4.2 Chamfering trials on aluminum workpieces

We conducted chamfering trials in aluminum work coupons with the same end-of-arm tool and observed a control behavior that was identical to the trials on titanium. For example, the positional error between the reference and the actual paths decreases gradually in each iteration as evident from Fig. 12a and b. After 13 passes, the positional error no longer reduces noticeably and reaches a saturation point as shown by the plots for absolute error. Generally, in our controller, if the tool cannot approach the initial reference trajectory in the first few passes, it leads to a gradual increase in normal forces in latter passes as observed from the trials involving titanium. When we plot the absolute error between the commanded and the actual robot trajectories for a few selected passes, as seen from Fig. 13a and b, we observe that the positional error between T_{CMD} and T_{ACT} is comparatively low in aluminum compared to the trials on titanium. As a consequence, the mean forces observed at each iteration tends to be relatively lower than the one observed during the titanium trials as depicted in Fig. 14a and b. At the initial iteration, the mean normal force is 1.42 N, while at 15th pass, it equals to 2.18 N. One explanation for the relatively low absolute error and the forces observed in chamfering aluminum coupons is due to the hardness of aluminum. As the hardness of aluminum is much lower than titanium, the robot's actual trajectory was able to approach the desired reference trajectory relatively fast in initial iterations, thus rendering the forces low in latter passes.

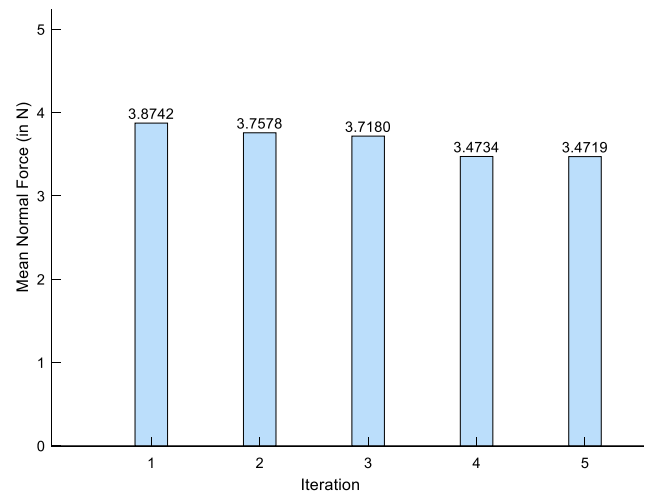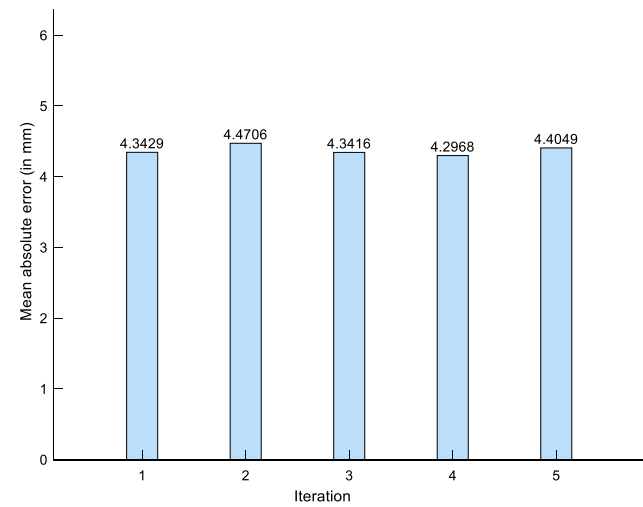**Table 3** The surface roughness of the chamfered workpiece

S. no	Roughness Ra (μm)		Reference roughness from literature (μm)	
	In titanium	In aluminum		
1	1.37	1.14	1.6 [49]	9.5 [15]
2	1.46	1.78		
3	1.47	1.83		

Fig. 15 Chamfered workpieces. **a** Titanium and **b** aluminum
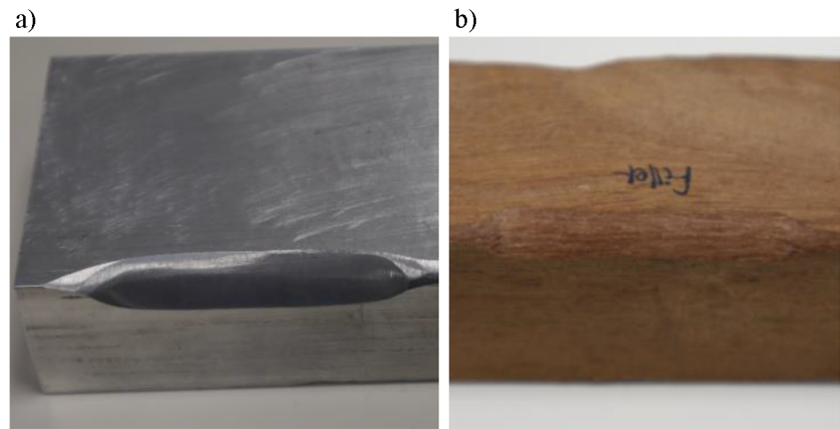

a)

b)

a)

b)

c)

d)

Fig. 16 **a** Mean absolute error, **b** mean normal force in filleting Aluminum, **c** mean absolute error, and **d** mean normal force in filleting wood

Fig. 18 Filleted workpieces. **a** Aluminum and **b** wood

a)   b)

4.3 Performance metric

To validate the chamfering trials on both titanium and aluminum coupons, we use the accuracy and the surface roughness as a performance metric to gauge the output. To measure the dimensions of the chamfered edges, we utilized a noncontact laser profile measurement device (GapGun Pro), and the measurements are shown in Table 2. In addition, the surface roughness of the chamfered edges is given in Table 3. As we utilized a coarse

Fig. 17 End-of-arm-tool for filleting wooden coupons

abrasive belt of grit size of P100 for the chamfering trials, an even finer surface finish can be achieved by using a finer abrasive, i.e., higher grit size.

We have obtained geometrical accuracy of ± 0.133 and ± 0.033 in the titanium and aluminum workpieces, respectively, which are acceptable for grinding operations in the industry [15, 48]. The chamfered output of the titanium and aluminum workpieces can be viewed from Fig.15a and b, respectively.

We have consistently obtained surface roughness values less than 1.5 (μm) in the titanium and 1.85 (μm) in aluminum workpieces, respectively, which are acceptable for grinding operations in the industry [48]. A further finer surface finish can be achieved by carrying out the experiments with abrasives of higher grit size and using coolants such as diamond polishing paste.
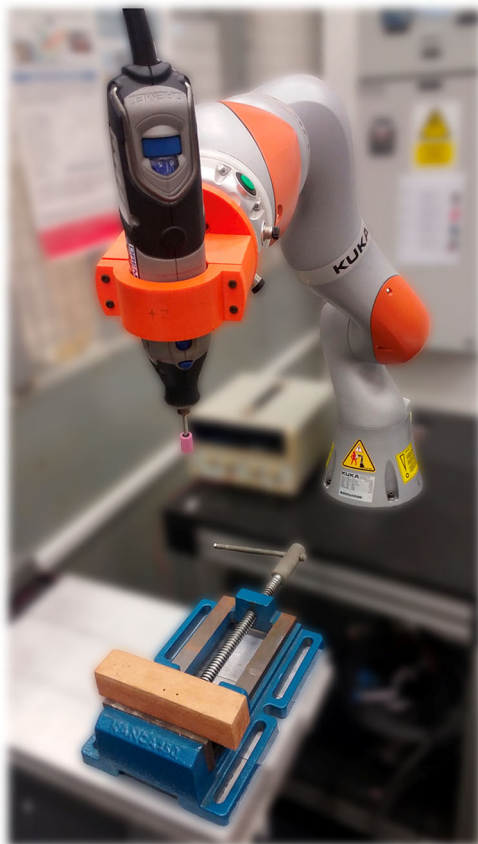
5 Experiments on filleting

To test the generalization of the iterative controller, we carried out filleting trials on the aluminum and wooden workpieces and briefly described the results in Section 5.1. Subsequently, the profile measurements of the filleted coupons are provided in Section 5.2.

Table 4 Profile measurement of filleted component*

S. no	Target filleting radius (in mm)	Actual radius (in mm)	
		In aluminum	In wood
1	5	5.53	5.26
2		5.37	4.95
3		5.41	6.12
Average		5.43	5.44

*These results have also been presented in [43]

5.1 Filleting trials on aluminum and wooden coupons

The filleting trials are carried out using a toolpath that is generated by the proposed mathematical model as seen in Fig. 5b with a user-specified fillet radius of 5 mm. The frequencies of the functions Y′ and θ are set to be 2 and 0.43, respectively, to ensure that the robot trajectory during the filleting follows a reciprocal movement for different angles of θ along the edge and not across it. Though the controller behavior in filleting is in general identical to the trials on chamfering, the absolute error between the reference and the actual filleting trajectories as well as the forces involved in filleting aluminum workpieces are relatively high compared to the chamfering trials on aluminum coupons as seen in the Fig. 16a and b, respectively. This observation of the relatively high mean absolute error may be owing to the several factors such as higher material removal, as the desired fillet radius is set to be 5 mm compared to 1 mm desired depth given in chamfering, as well as the complicated trajectory of the filleting itself. From the experiments, the mean normal force in the first iteration is observed to be 7.35 N and gradually adapted to 5.8 N in the final iteration. A sample of the fillet output in aluminum work coupon can be seen in Fig. 18a.

For the filleting trials on wooden workpieces, we have utilized Dremel E-4000 as the end-of-arm tool (EOAT) as observed in Fig. 17 due to its suitability. Apart from EOAT and the abrasives used, the remaining setup and the procedure followed is same as the filleting trials on aluminum. In the trials, we observed that the mean absolute error and mean normal force in each iteration to be relatively low compared to the filleting trials on aluminum as shown in Fig. 16c and d, respectively. A sample specimen of the filleted component can be viewed in Fig. 18b.

5.2 Performance metric of the filleted components

To validate the output of the filleted components, we use the accuracy of the filleted component using a noncontact profile measurement device (GapGun Pro). The readings from the device are shown in Table 4 for several trials on both aluminum and wooden workpieces. These results are acceptable for filleting in the industrial applications as they are within ± 1 mm tolerance of desired filleting profile [48].

6 Conclusion and future work

In this paper, we have presented an adaptive framework to carry out the finishing process in a variety of materials, using a collaborative robot utilizing an iterative impedance control architecture and kinesthetic teaching. In addition, we proposed a mathematical model based on Lissajous curves to generate complex filleting toolpath in real time. The experiments on both chamfering and filleting processes prove that the proposed iterative controller based on impedance can obtain desired geometric profile and surface finish for various materials. Our controller requires no prior knowledge of the forces required to polish a material as the position and forces are adapted simultaneously based on iterative feedback. Due to its iterative adaptation, our controller reduces the amount of rework needed and thus is highly suitable for SMEs that handle the high volume and low mix parts. Furthermore, our framework is inexpensive since it requires no additional vision and force sensors while overcoming the problems associated with manual programming. We acknowledge that for tasks involving complex geometries such as the finishing of fan blades and turbines parts, we will need to generate and adapt trajectories on the free-form surfaces. To that end, we plan to integrate the iterative learning controller with the trajectory generating method proposed by Kana et al. [50] in the future work.

References

1. Kazerooni H, Houpt PK, Sheridan TB (1986) Robust compliant motion for manipulators, part II: design method. IEEE J Robot Autom 2:93–105. https://doi.org/10.1109/JRA.1986.1087047

2. Chiaverini S, Sciavicco L (1993) The parallel approach to force/position control of robotic manipulators. IEEE Trans Robot Autom 9:361–373. https://doi.org/10.1109/70.246048

3. Mohammad AEK, Hong J, Wang D, Guan Y (2019) Synergistic integrated design of an electrochemical mechanical polishing end-effector for robotic polishing applications. Robot Comput Integr Manuf 55:65–75. https://doi.org/10.1016/j.rcim.2018.07.005

4. Buckmaster DJ, Newman WS, Somes SD (2008) Compliant motion control for robust robotic surface finishing. In: Proc World Congr Intell Control Autom, pp 559–564. https://doi.org/10.1109/WCICA.2008.4592983

5. Arunachalam APS, Idapalapati S, Subbiah S (2015) Multi-criteria decision making techniques for compliant polishing tool selection. Int J Adv Manuf Technol 79:519–530. https://doi.org/10.1007/s00170-015-6822-y

6. Tsai MJ, Huang JF (2006) Efficient automatic polishing process with a new compliant abrasive tool. Int J Adv Manuf Technol 30:817–827. https://doi.org/10.1007/s00170-005-0126-6

7. Huissoon JP, Ismail F, Jafari A, Bedi S (2002) Automated polishing of die steel surfaces. Int J Adv Manuf Technol 19:285–290. https://doi.org/10.1007/s001700200036

8. Roswell A, Xi F, Liu G (2006) Modelling and analysis of contact stress for automated polishing. Int J Mach Tools Manuf 46:424–435. https://doi.org/10.1016/j.ijmachtools.2005.05.006

9. Hu L, Zhan J (2015) Study on the orthomogonalization for hybrid motion/force control and its application in aspheric surface

polishing. Int J Adv Manuf Technol 77:1259–1268. https://doi.org/10.1007/s00170-014-6499-7

10. Tian F, Li Z, Lv C, Liu G (2016) Polishing pressure investigations of robot automatic polishing on curved surfaces. Int J Adv Manuf Technol 87:639–646. https://doi.org/10.1007/s00170-016-8527-2

11. Huang H, Gong ZM, Chen XQ, Zhou L (2002) Robotic grinding and polishing for turbine-vane overhaul. J Mater Process Technol 127:140–145. https://doi.org/10.1016/S0924-0136(02)00114-0

12. Pessoles X, Tournier C (2009) Automatic polishing process of plastic injection molds on a 5-axis milling center. J Mater Process Technol 209:3665–3673. https://doi.org/10.1016/j.jmatprotec.2008.08.034

13. Huang H, Gong ZM, Chen XQ, Zhou L (2003) SMART robotic system for 3D profile turbine vane airfoil repair. Int J Adv Manuf Technol 21:275–283. https://doi.org/10.1007/s001700300032

14. Mohammad AEK, Hong J, Wang D (2018) Design of a force-controlled end-effector with low-inertia effect for robotic polishing using macro-mini robot approach. Robot Comput Integr Manuf 49:54–65. https://doi.org/10.1016/j.rcim.2017.05.011

15. Bone GM, Elbestawi MA, Lingarkar R, Liu L (1991) Force control for robotic deburring. J Dyn Syst Meas Control Trans ASME 113:395–400. https://doi.org/10.1115/1.2896423

16. Li J, Zhang T, Liu X, Guan Y, Wang D (2018) A Survey of robotic polishing, 2018 IEEE Int. Conf. Robot. Biomimetics. ROBIO 2018:2125–2132. https://doi.org/10.1109/ROBIO.2018.8664890

17. Siciliano B, Villani L (1999) Robot force control, robot force control. https://doi.org/10.1007/978-1-4615-4431-9

18. Zeng G, Hemami A (1997) An overview of robot force control. Robotica. 15:473–482. https://doi.org/10.1017/S026357479700057X

19. Hsu FY, Fu LC (2000) Intelligent robot deburring using adaptive fuzzy hybrid position/force control. IEEE Trans Robot Autom 16:325–335. https://doi.org/10.1109/70.864223

20. D. Surdilovic, H. Zhao, G. Schreck, J. Krueger, Advanced methods for small batch robotic machining of hard materials, Robot. Proc. Robot. 2012; 7th Ger. Conf. (2012) 1–6

21. Surdilovic D (1996) Contact stability issues in position based impedance control: theory and experiments. Proc - IEEE Int Conf Robot Autom 2:1675–1680. https://doi.org/10.1109/robot.1996.506953

22. Hogan N (1985) Impedance control: an approach to manipulation: part III-applications. J Dyn Syst Meas Control Trans ASME 107:17–24. https://doi.org/10.1115/1.3140701

23. Kazerooni H, Bausch JJ, Kramer BM (1986) An approach to automated deburring by robot manipulators. J Dyn Syst Meas Control Trans ASME 108:354–359. https://doi.org/10.1115/1.3143806

24. W. Xianlun, W. Yong, X. Yunna, Adaptive control of robotic deburring process based on impedance control, 2006 IEEE Int. Conf. Ind. Informatics, INDIN'06. (2006) 921–925. https://doi.org/10.1109/INDIN.2006.275700

25. Bonilla I, Mendoza M, González-Galván EJ, Chávez-Olivares C, Loredo-Flores A, Reyes F (2012) Path-tracking maneuvers with industrial robot manipulators using uncalibrated vision and impedance control. IEEE Trans Syst Man Cybern Part C Appl Rev 42:1716–1729. https://doi.org/10.1109/TSMCC.2012.2218235

26. Roveda L, Vicentini F, Pedrocchi N, Tosatti LM (2015) Impedance control based force-tracking algorithm for interaction robotics tasks: an analytically force overshoots-free approach, ICINCO 2015 - 12th Int. Conf Informatics Control Autom Robot Proc 2:386–391. https://doi.org/10.5220/0005565403860391

27. Li Y, Ganesh G, Jarrasse N, Haddadin S, Albu-Schaeffer A, Burdet E (2018) Force, impedance, and trajectory learning for contact tooling and haptic identification. IEEE Trans Robot 34:1170–1182. https://doi.org/10.1109/TRO.2018.2830405

28. Ting W, Aiguo S (2019) An adaptive iterative learning based impedance control for robot-aided upper-limb passive rehabilitation. Front Robot AI 6:1–11. https://doi.org/10.3389/frobt.2019.00041

29. Li RJ, Han ZZ (2005) Survey of iterative learning control. Kongzhi Yu Juece/Control Decis 20:961–966. https://doi.org/10.1109/mcs.2006.1636313

30. Cheah CC, Wang D (1998) Learning impedance control for robotic manipulators. IEEE Trans Robot Autom 14:452–465. https://doi.org/10.1109/70.678454

31. Wang D, Cheah CC (1998) An iterative learning-control scheme for impedance control of robotic manipulators. Int J Robot Res 17:1091–1104. https://doi.org/10.1177/027836499801701006

32. Li X, Liu YH, Yu H (2018) Iterative learning impedance control for rehabilitation robots driven by series elastic actuators. Automatica. 90:1–7. https://doi.org/10.1016/j.automatica.2017.12.031

33. Pan Z, Zhang H (2007) Analysis and suppression of chatter in robotic machining process, ICCAS 2007 - Int. Conf Control Autom Syst:595–600. https://doi.org/10.1109/ICCAS.2007.4407093

34. Zhang Z, Guo D, Wang B, Kang R, Zhang B (2015) A novel approach of high speed scratching on silicon wafers at nanoscale depths of cut. Sci Rep 5:1–9. https://doi.org/10.1038/srep16395

35. Zhang Z, Huang S, Wang S, Wang B, Bai Q, Zhang B, Kang R, Guo D (2017) A novel approach of high-performance grinding using developed diamond wheels. Int J Adv Manuf Technol 91:3315–3326. https://doi.org/10.1007/s00170-017-0037-3

36. Cui J, Zhang Z, Jiang H, Liu D, Zou L, Guo X, Lu Y, Parkin IP, Guo D (2019) Ultrahigh recovery of fracture strength on mismatched fractured amorphous surfaces of silicon carbide. ACS Nano 13:7483–7492. https://doi.org/10.1021/acsnano.9b02658

37. Wang B, Zhang Z, Chang K, Cui J, Rosenkranz A, Yu J, Te Lin C, Chen G, Zang K, Luo J, Jiang N, Guo D (2018) New deformation-induced nanostructure in silicon. Nano Lett 18:4611–4617. https://doi.org/10.1021/acs.nanolett.8b01910

38. Zhang Z, Cui J, Wang B, Wang Z, Kang R, Guo D (2017) A novel approach of mechanical chemical grinding. J Alloys Compd 726:514–524. https://doi.org/10.1016/j.jallcom.2017.08.024

39. Zhang Z, Shi Z, Du Y, Yu Z, Guo L, Guo D (2018) A novel approach of chemical mechanical polishing for a titanium alloy using an environment-friendly slurry. Appl Surf Sci 427:409–415. https://doi.org/10.1016/j.apsusc.2017.08.064

40. Zhang Z, Wang B, Kang R, Zhang B, Guo D (2015) Changes in surface layer of silicon wafers from diamond scratching. CIRP Ann - Manuf Technol 64:349–352. https://doi.org/10.1016/j.cirp.2015.04.005

41. Chong JWS, Ong SK, Nee AYC, Youcef-Youmi K (2009) Robot programming using augmented reality: an interactive method for planning collision-free paths. Robot Comput Integr Manuf 25:689–701. https://doi.org/10.1016/j.rcim.2008.05.002

42. Pan Z, Polden J, Larkin N, Van Duin S, Norrish J (2012) Recent progress on programming methods for industrial robots. Robot Comput Integr Manuf 28:87–94. https://doi.org/10.1016/j.rcim.2011.08.004

43. Lakshminarayanan S, Manyar OM, Campolo D (2020) Toolpath generation for robot filleting. Lect Notes Mech Eng:273–280. https://doi.org/10.1007/978-981-15-0054-1_28

44. Ficuciello F, Villani L, Siciliano B (2015) Variable impedance control of redundant manipulators for intuitive human-robot physical interaction. IEEE Trans Robot 31:850–863. https://doi.org/10.1109/TRO.2015.2430053

45. Heinrichs B, Sepehri N, Thornton-Trump AB (1996) Position-based impedance control of an industrial hydraulic manipulator. Proc - IEEE Int Conf Robot Autom 1:284–290. https://doi.org/10.1109/robot.1996.503791

46. WORLD SCIENTIFIC (2009) Control of Robots in Contact Tasks: A Survey. In: Dynamic. Robust control robot. Interact, pp 1–76. https://doi.org/10.1142/9789812834768_0001
47. Jayaweera N, Webb P (2010) Measurement assisted robotic edge deburring of aero engine components. WSEAS Trans Syst Control 5:174–183
48. Malkin S, Guo C (2008) Grinding technology: theory and application of machining with abrasives. Industrial Press Inc., NewYork
49. de Mello AV, de Silva RB, Machado ÁR, Gelamo RV, Diniz AE, de Oliveira RFM (2017) Surface grinding of Ti-6Al-4V alloy with SiC abrasive wheel at various cutting conditions. Procedia Manuf 10:590–600. https://doi.org/10.1016/j.promfg.2017.07.057
50. Kana S, Tee KP, Campolo D (2021) Human–robot co-manipulation during surface tooling: a general framework based on impedance control, haptic rendering and discrete geometry. Robot Comput Integr Manuf 67:102033. https://doi.org/10.1016/j.rcim.2020.102033